Behaviour of niobium during early Earth's differentiation: insights from its local structure and oxidation state in silicate melts at high pressure

C. Sanloup, B. Cochain, C de Grouchy, K. Glazyrin, Z Konôpkova, H-P Liermann, I. Kantor, R Torchio, O. Mathon, T. Irifune

Behaviour of niobium during early Earth's differentiation: insights from its local structure and oxidation state in silicate melts at high pressure

C Sanloup[1], B Cochain[1], C de Grouchy[2], K Glazyrin[3], Z Konôpkova[3], H-P Liermann[3], I Kantor[4]‡, R Torchio[4], O Mathon[4], T Irifune[5]

[1] Sorbonne Université, CNRS-INSU, Institut des Sciences de la Terre Paris, ISTeP UMR 7193, F-75005 Paris, France
[2] Scottish Universities Physics Alliance (SUPA), and Centre for Science at Extreme Conditions, School of Physics and Astronomy, University of Edinburgh, Edinburgh, EH9 3FD, UK
[3] Photon Science DESY, D-22607 Hamburg,Germany
[4] European Synchrotron Radiation Facility, 71 Avenue des Martyrs, F-38043 Grenoble, France
[5] GRC, Ehime University, Ehime 790-8577, Japan

E-mail: chrystele.sanloup@upmc.fr

Abstract. Niobium (Nb) is one of the key trace elements used to understand Earth's formation and differentiation, and is remarkable for its deficiency relative to tantalum in terrestrial rocks compared to the building chondritic blocks. In this context, the local environment of Nb in silica-rich melts and glasses is studied by *in situ* X-ray absorption spectroscopy (XAS) at high pressure (P) up to 9.3 GPa and 1350 K using resistive-heating diamond-anvil cells. Nb is slightly less oxidized in the melt (intermediate valence between +4 and +5) than in the glass (+5), an effect evidenced from the shift of the Nb-edge towards lower energies. Changes in the pre-edge features are also observed between melt and glass states, consistently with the observed changes in oxidation state although likely enhanced by temperature (T) effects. The oxidation state of Nb is not affected by pressure neither in the molten nor glassy states, and remains constant in the investigated P-range. The Nb-O coordination number is constant and equal to 6.3 ± 0.4 below 5 GPa, and only progressively increases up to 7.1 ± 0.4 at 9.3 GPa, the maximum P investigated. If these findings were to similarly apply to basaltic melts, that would rule out the hypothesis of Nb/Ta fractionation during early silicate Earth's differentiation, thus reinforcing the alternative hypothesis of fractionation during core formation on reduced pre-planetary bodies.

‡ Present address: Technical University of Denmark, Department of Physics, 2800 Kgs. Lyngby, Denmark.

1. Introduction

Niobium (Nb) is a high field strength element (HFSE) due to its small size and high charge. Nb can occur as Nb^{2+}, Nb^{4+}, and Nb^{5+} oxides under ambient conditions, while Nb^{5+} is the only oxidation state present in geological minerals. It is of geochemical interest due to what is termed the 'missing niobium' or 'niobium paradox'. The ratio of Nb to Ta and La for the crust, depleted mantle, and ocean island basalts is less than expected for a chondritic Earth [1]. This has been used to infer the presence of a hidden Nb-rich, or super-chondritic, reservoir. Potential reservoirs have been proposed such as subducted eclogite (e.g. [2]), an early enriched crustal reservoir derived from a Hadean magma ocean and subducted to the D" layer [3], and the Earth's core [4]. Preferential sequestration of Nb over Ta in the core could indeed be a consequence of Nb valence change in silicate melts during core formation upon decreasing fO_2 conditions as inferred from metal/silicate partitioning experiments [5, 6]. This latter hypothesis is supported by recent analysis of silicate meteorites from various asteroidal parent bodies, with the most reduced ones having lower Nb/Ta ratios [7]. The accretion of such bodies on the growing Earth's would explain its subchondritic Nb/Ta signature, assuming that full core/mantle re-equilibration was not attained.

The former hypothesis of Nb sequestration in an early enriched crustal reservoir might be tested by exploring the effect of pressure on the local structure of Nb in melts. Indeed, structural changes in silicate melts affect their physical properties, but they may also affect their chemical properties and the way elements partition between the melt and crystals upon partial melting of a source mantle rock. Links between melt structure and crystal/melt element partitioning have been explored theoretically at ambient pressure for some trace elements (e.g. [8] and references therein). At high pressure, lutetium (Lu) was shown experimentally to undergo a change of coordination number circa 4-5 GPa in basaltic melts, a change that underpins the evolution of Lu mineral/melt partitioning at high pressure [9], and consequently the evolution of the Lu/Hf ratio in terrestrial rocks depending on the melting depth. In the case of Nb, previous XAS studies in silicate glasses at ambient conditions were initially focused on continental crust analogues (sodium disilicate NS2, sodium trisilicate NS3, and haplogranitic glasses), and found that Nb is present as NbO_6 moiety with a +5 valence [10]. The range of compositions and fO_2 conditions was later extended to Fe-free mafic glasses between iron-wüstite (IW)-4.3 to IW+6.7, but no valence change was observed [11]. Only at IW-7.9 was Nb found in +2 valence in a silicate glass that had been previously equilibrated with molten Fe-alloy at 5 GPa [12]. Quench effects might however occur, and the only *in situ* XAS study on Nb environment in a granitic melt, using a hydrothermal diamond-anvil cell at 0.7 GPa-983 K, also shows a coordination number of 6 in both glass and melt, while no information is given on Nb oxidation state [13]. Here we use X-ray Absorption Near Edge Structure (XANES) and Extended X-Ray Absorption Fine Structure (EXAFS) spectroscopies with resistive heating diamond anvil cells (RH-DAC) to determine the oxidation states of Nb and its coordination and oxygen distance in silicate melts at high

pressure and temperature.

2. Samples and high pressure XAS data acquisition

The haplogranite (HPG) composition was chosen as a simplified analogue of the continental crust. The HPG glass was synthesized by mixing together the appropriate amounts of chemical grades (SiO_2, Al_2O_3, K_2CO_3, Na_2CO_3) from Alfa Aesar with purity >99.99% (Table 1). The mixed powders were ground and decarbonated for 12 hours at 1273 K, then fused at 1873 K in a platinum crucible for 1 hour. The molten glass was quenched by immediately placing the crucible into cold water. The glass was then ground and remelted twice to ensure chemical homogeneity and finally checked for lack of crystals and bubbles. The composition of the glass (Table 1) was determined by taking an average over 10 analyses made with a CAMECA SX100 electron microprobe at the EMMAC centre (The Edinburgh Materials and Micro-Analysis Centre), University of Edinburgh. The microprobe analyses were performed under soft operating conditions, in order to avoid any loss of Na, with a 15 kV accelerating voltage, a defocused beam of $10\,\mu m$ and a current of 15 nA. Nb was added in the form of high purity Nb_2O_5 to the ground glass to match a 0.5 at% Nb content (3.75 wt% Nb). Approximately 10 wt% water was added to the sample through high pressure addition in a piston-cylinder press at 2 GPa and 1670 K in order to lower the melting temperature to temperatures achievable in a resistively heated diamond anvil cell. The samples were crushed to a fine homogeneous powder before being loaded. XAS measurements at ambient and high pressure-high temperature (high *P-T*) conditions were performed in transmission mode across the Nb-K edge (18.97 keV) on the BM23 beamline at the European Synchrotron Radiation Facility (ESRF - Grenoble, France). Details of the beamline layout are reported elsewhere [14]. The storage ring was operating in the 16-bunch mode with an average current of 200 mA. X-rays were generated using a bending magnet, and monochromatized with a double-crystal, fixed exit Si(111) monochromator. The beamsize was 0.1×0.3 mm^2. The energy of the EXAFS spectra was calibrated using a Nb metallic foil and no significant drift of the energy was observed for the duration of the measurements. EXAFS spectra of the Nb-bearing reference compounds (Nb_2O_5 and NbO_2), the Nb-doped HPG glass and the in situ EXAFS spectra measurements were recorded in transmission from 18800 eV to 19846 eV with a total scan time of about 20 minutes. EXAFS spectra of the melt were measured under high *P-T* conditions of up to 9.3 GPa and 1350 K using resistive heating diamond-anvil cell under vacuum conditions [15]. We used nano-polycrystalline diamond anvils of $400\,\mu m$ culets synthesized at the Geodynamics Research Center (Ehime University, Japan) instead of single crystal diamond anvils in order to eliminate the serious interference of the diamond Bragg peaks in the EXAFS spectra [16]. High *T* was achieved by resistive heating through a graphite heater. Temperature was recorded by two R-type thermocouples (thermally insulated from the diamond anvils) placed on both sides of the gasket indent as close to the sample chamber as possible. Finely ground Nb-HPG sample powder was loaded into the $250\,\mu m$

Table 1. Compositions from electron microprobe analysis of the starting HPG glass given in wt% oxide. Analyses are based on an average of 10 sample spots, standard deviations are shown in brackets.

Oxide	Sample
SiO_2	78.7 (3)
Al_2O_3	11.9 (2)
Na_2O	3.3 (3)
K_2O	3.7 (1)
Total	99.4 (5)

electro-eroded hole of the rhenium gasket, along with a ruby sphere and a Pt foil inserted on the side of the sample chamber for P calibration. The powder was packed into the hole thoroughly to avoid collapse of the sample chamber. Experiments were conducted by cold compression of the sample to a given pressure, followed by gradual heating to the desired temperature between 1200 K and 1350 K. Diffraction on the Pt calibrant was collected for 300 s at each pressure point before and during heating using a MAR165 CCD detector. P was determined before and during the experiment by monitoring ruby fluorescence and the cell volume of Pt [17]. Estimated error bars are ± 0.5 GPa on P, and ± 50 K on T. Before recording the EXAFS spectra, the molten state of the sample was assessed by the disappearance of crystalline Bragg peaks in the diffraction patterns and concomitant appearance of diffused scattered signal by the melt. All melt spectra were collected between 1270 K and 1350 K. X-ray diffraction spectra of the sample were systematically recorded before and after collection of EXAFS data to check for the lack of crystallization.

3. EXAFS data analysis

The extended X-ray absorption fine structure (EXAFS) signal (χ) was extracted using the DEMETER package based on the IFEFFIT program [18]. Briefly, an average of 4 to 6 EXAFS spectra was normalized to the absorption edge height using the background algorithm from the DEMETER package with the minimum atom-atom contact distance, R_{bkg}, chosen as 1.3 Å. The edge E_0 was calculated as the first maximum of the first derivative of the absorption spectra. EXAFS interference functions $k^2\chi(k)$ were exported into ARTEMIS, Fourier transformed and fit to the EXAFS equation [19] over k-range of $2.25-12$ Å^{-1} for the crystalline references, and $2.5-8.5$ Å^{-1} for the glasses at ambient conditions and the melts at high P-T conditions. For all compositions, the fit parameters included the number of oxygen neighboring atoms, CN, average distance, d, to the central Nb atom, the Debye-Waller factor, σ^2, characterizing the degree of disorder present in the signal, the amplitude reduction factor S_0^2 and the energy offset

Table 2. EXAFS-derived structural parameters for the crystalline reference NbO_2 and for the parent glass at room temperature (R), the melts (M) and the quenched glasses (Q).

	P (GPa)	Nb-O CN	d (Å)	R-factor	σ^2	ΔE_0
NbO_2	Ambiant	6.01(30)	2.09(8)	0.07	0.010(2)	1.24(37)
R	1.0	6.4(1)	2.00(2)	0.08	0.010(2)	-0.18(24)
M	1.0	6.1(2)	1.96(3)	0.12	0.010(2)	-0.75(45)
R	3.0	6.3(1)	1.99(1)	0.07	0.010(2)	1.22(75)
M	3.0	6.4(2)	1.98(2)	0.26	0.120(2)	1.05(43)
Q	3.0	6.1(2)	1.97(3)	0.09	0.010(2)	1.64(38)
R	4.3	6.2(3)	1.98(2)	0.06	0.010(2)	1.24(32)
M	4.3	6.3(3)	1.93(6)	0.09	0.040(2)	1.66(93)
Q	4.3	5.8(1)	1.95(5)	0.07	0.010(2)	1.47(37)
R	7.5	6.4(2)	2.00(4)	0.08	0.010(2)	1.80(95)
M	7.5	6.8(2)	1.93(7)	0.13	0.080(2)	1.31(1.01)
R	9.3	6.4(3)	1.99(4)	0.07	0.010(2)	2.07(65)
M	9.3	7.1(4)	1.93(4)	0.09	0.050(2)	1.87(87)

ΔE_0 (Table 2). The amplitude reduction factor S_0^2 was fit for the reference NbO_2 EXAFS spectrum, and set to the best fit value found, i.e. 0.73 ± 0.09, for the other spectra to minimize errors and correlation between the derived structural parameters. The fitted values of ΔE_0 never exceed 4 eV confirming the validity of the fitting procedure. Finally, the third order anharmonic cumulant-expansion fitting parameter, σ^3, which measures the asymmetry in the signal disorder, was included in the fitting of the melts EXAFS spectra in order to partially compensate for the structural disorder due to the high P-T conditions but did not improve the fitting results and is therefore not presented here. The goodness of the fits is expressed by the R-factor which is a sum-of-squares of the fractional misfit between model and EXAFS data [20].

4. Results and discussion

Nb K-edge XANES spectra of the starting glass at high pressure and room temperature (R), in the melt at high pressure (M) and the resulting quench at high pressure (Q), and of the Nb_2O_5 and NbO_2 references are shown in Fig.1.

The XANES spectra of the references show a clear difference in the edge position with the inflexion point E_0 of the Nb^{5+} reference Nb_2O_5 being at 19004.05 eV while the one of the Nb^{4+} reference NbO_2 lies almost 3 eV below at 19001.35 eV, highlighted in Fig. 2. Overall, the sample spectra bear close resemblance to those of the alkali niobosilicate crystals (vuonnemite and labuntsovite) and glasses presented in [10], for which Nb is
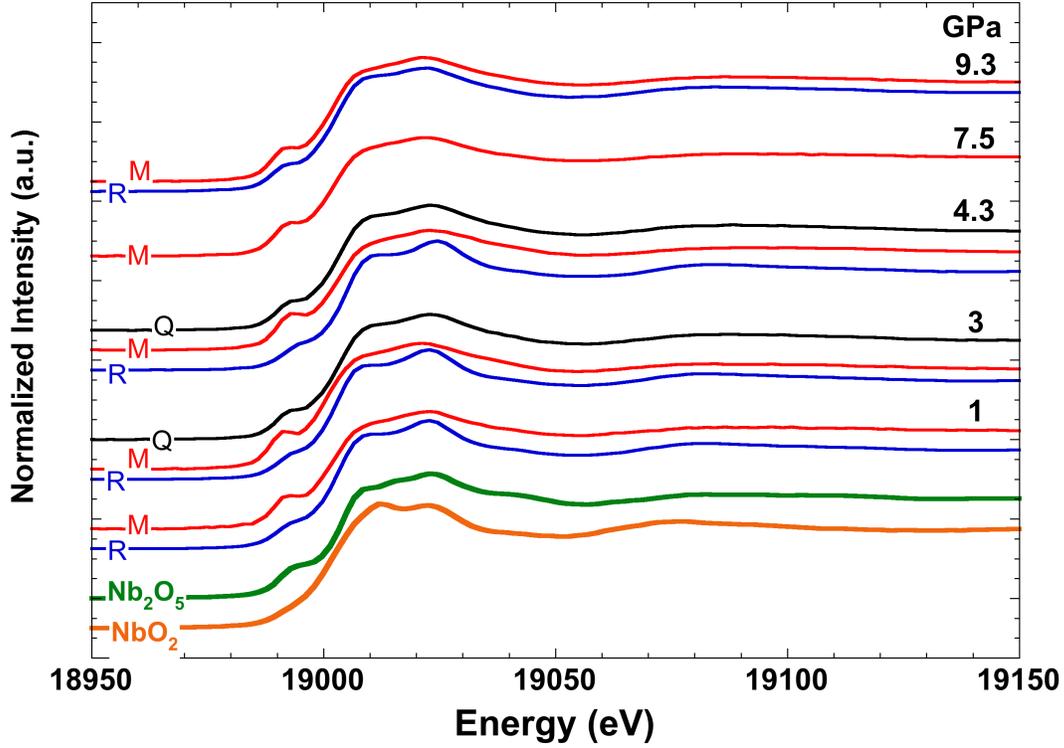
Figure 1. Normalized XAS spectra for the references and for the pressurized glasses before heating (blue), high pressure melts collected at T ranging between 1270 K and 1350 K (red), and corresponding quenched glasses (black) at all P points investigated.

pentavalent and coordinated to 6 oxygen atoms. All glasses show a doublet in the main edge (Fig.1), similar to those for the silicate glasses [10] and for 6-coordinated Zr in synthetic glasses [21, 22]. These features tend to disappear in the melt in agreement with a disordered local structure at high temperature as observed by [13] at 0.7 GPa for Nb. The pre-edge resolution and white line components exhibit small but clear differences between the melts and glasses, either before or after heating as shown in Figs. 1 and 2a, and at the exception of the pre-edge features at 9.3 GPa where no change is observed. The first derivative of the XANES spectra, from which is determined the position of the inflexion point of the white line in-situ XANES data are shown in Fig. 2. The inflexion point of the glasses located at 19003.3 ± 0.2 eV shows that Nb is in 5+ state, and is not affected by the increase in pressure. The inflexion point of the white line of the melt XANES spectra are found to be systematically at a lower position by 0.8 eV to 1.2 eV than for the glasses (Fig. 2b). Temperature-induced modifications are not expected to induce such a shift, as only 0.15 eV difference was observed between melt and glass at the Ni K-edge [23]. Instead, the shift of the edge indicates that Nb is found in a lower redox state in the melt closer to +4 compared to the glass. As for the changes affecting the pre-edge peak, its intensity is lower and its position shifted
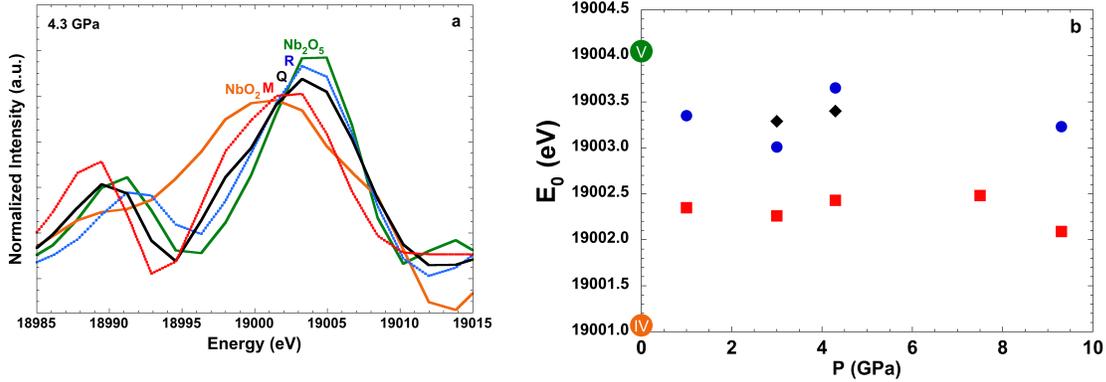
Figure 2. (a) XANES derivative spectra for the references and for the starting glass, high pressure melt, and high pressure quenched glass at 4.3 GPa. (b) Position of the Nb-edge as measured by the inflexion point (blue circles: glass before heating, red squares: melt, black diamonds: quenched glass after heating). 'IV' represents the E_0 value of NbO_2 (+4 valence), 'V' the E_0 value of Nb_2O_5 (+5 valence).

to higher energies in the glass compared to the melt, as previously reported for Fe, Ti and Ni (see [24] and references therein), and consistently with the increased oxidation state in the glass. These changes may also be enhanced by temperature, as theoretically understood through increased radial distortions and deviations from central symmetry of the local environment [25]. Only at the highest P point (i.e. 9.3 GPa) have the room T glass and melt comparable pre-edge features. This could be due to the opposite effects of increased CN [26] and decreased oxidation state that could cancel each other out.Finally, subtle differences in pre-edge features between room T and quenched glasses might be attributed to structural relaxation effects that occurred during melting, although this can be treated with caution as we only have 2 P points for which both room T and quenched glasses data were collected (at 3.0 GPa and 4.3 GPa).

The best model for each EXAFS spectrum is presented on Fig. 3a. The normalized k^2-weighted spectra and their Fourier Transform for the samples at 4.3 GPa and for the NbO_2 reference are shown in Fig.3, and the corresponding fit parameters are listed in Table 2. Small differences are observed between the in-situ samples and the oxide model compounds, notably at high k. One main contribution is detected around the Nb atom (Fig.3b).

Up to 4.3 GPa, this Nb-O shell has 5.8 to 6.3 nearest neighbors (Fig.4a) and an average bond-length of 2.00 Å, 1.95 Å and 1.95 Å respectively for the starting glasses, the melts and the high pressure quenched glasses at the pressure investigated (Fig.4b). Our results for these low P glasses and melts agree with ambient P data on similar glasses [10]. For the two highest P points, i.e. 7.5 GPa and 9.3 GPa, the number of nearest oxygen neighbors increases up to 7.1±0.4. No concomitant increase of the Nb-O distance is observed (Fig. 4b), but that could be due to the larger error bars (±0.7 Å) of the fit at high pressures.
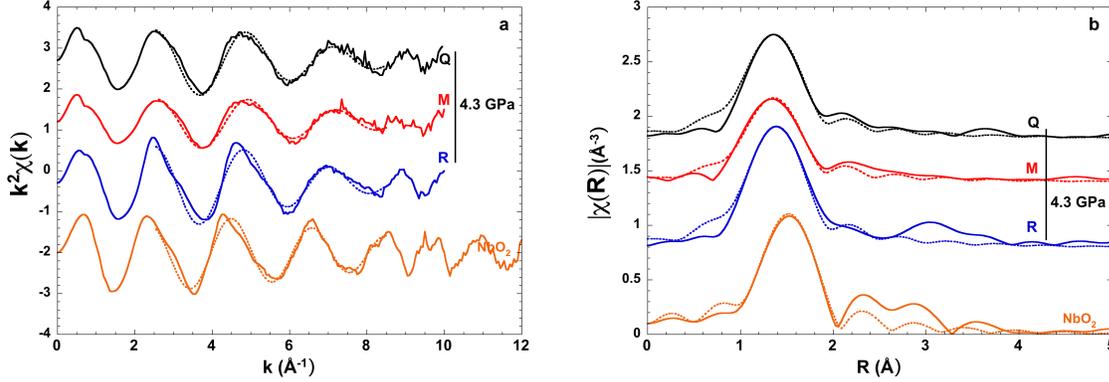
Figure 3. (a) Normalized, k^2-weighted, EXAFS spectra for the references and sample at 4.3 GPa (colors: same as for other figures; full lines: data, dashed lines: fit). (b) Fourier Transform of the corresponding normalized, k^2-weighted, EXAFS spectra.
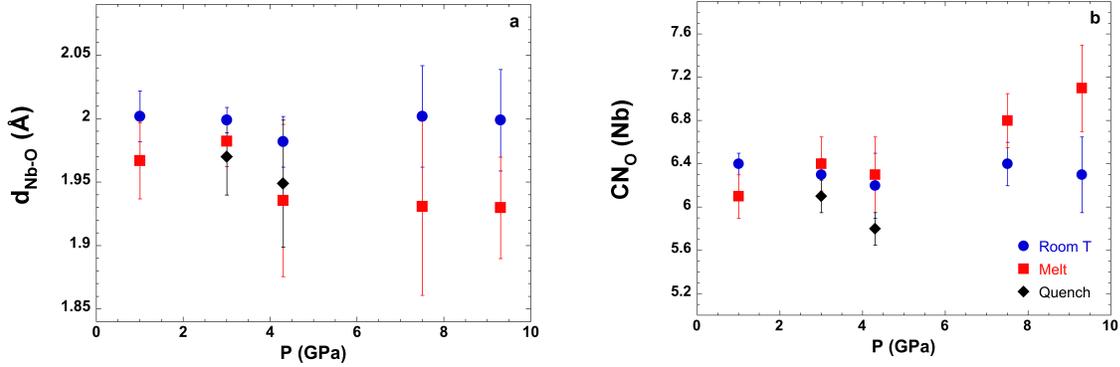
Figure 4. (a) Fitted Nb-O interatomic distance. (b) Fitted Nb-O coordination number.

5. Implications

Early silicate Earth's differentiation events, i.e. mantle melting, are likely to have occurred at pressures lower than 7 GPa where structural changes of Nb in haplogranitic melts are negligible. If these results were to apply to basaltic melts as well, this would rule out the hypothesis of Nb/Ta fractionation through the formation of enriched silicate reservoirs at depth. Nb local structure and oxidation state remain to be investigated in basaltic melts at high pressures, as Lu local environment was shown by *in situ* X-ray diffraction to be not affected by P in continental crustal melts, but to drastically change coordination number from 6 to 8 in basaltic melts circa 4-5 GPa [9]. The relevant experiments are nonetheless challenging due to the high melting point of basalts especially at high P, combined with the weakening of EXAFS oscillations at high T. Rutile-melt Nb partitioning data with silica-rich melts analogous to the one studied here have only been collected up to 3.5 GPa [27]. They did not show any P-effect on Nb partitioning, which is consistent with the absence of changes in the local environment of Nb, includ-

ing coordination number and oxidation state, in silica-rich melts over this P-range as reported here. The P-range investigated for partitioning experiments might have been too small to evidence any clear P dependence. Rutile-basaltic melt partitioning data collected up to 10 GPa [28] have evidenced a marked decrease of the rutile-melt partition coefficient for Nb, $D_{rutile/melt}$, with increased P, which was interpreted as resulting from structural changes in the melt as the rutile-TiO_2(II) phase transition only occurs circa 7 GPa. Structural changes in the melt might however concern either a change of the local environment around Nb atoms, as reported here for silica-rich melts with the observed increase of Nb-O coordination number at the highest P points, and/or a change in the melt bulk properties such as the compressibility. The latter, for instance, has been invoked to explain the change in REE partitioning between olivine and silicate melt at high pressure [29].

Acknowledgements

References

[1] C. Munker. Evolution of planetary cores and the Earth-Moon system from Nb/Ta systematics. *Science*, 301:84–87, 2003.

[2] R. L. Rudnick. Rutile-bearing refractory eclogites: Missing link between continents and depleted mantle. *Science*, 287:278–281, 2000.

[3] O. Nebel, W. van Westrenen, P. Z. Vroon, M. Wille, and M. M. Raith. Deep mantle storage of the Earths missing niobium in late-stage residual melts from a magma ocean. *Geochim. Cosmochim. Acta*, 74:4392–4404, 2010.

[4] J. Wade and B. J. Wood. The Earths missing niobium may be in the core. *Nature*, 409:75–78, 2001.

[5] B. J. Wood, J. J. Wade, and M. R. Kilburn. Core formation and the oxidation state of the Earth: Additional constraints from Nb, V and Cr partitioning. *Geochim. Cosmochim. Acta*, 72:1415–1426, 2008.

[6] C. Cartier, T. Hammouda, M. Boyet, M. A. Bouhifd, and J.-L. Devidal. Redox control of the fractionation of niobium and tantalum during planetary accretion and core formation. *Nature Geo.*, 7:573–576, 2014.

[7] C. Munker, R.O.C. Fonseca, and T. Schulz. Silicate Earth's missing niobium may have been sequestered into asteroidal cores. *Nature Geosci.*, 10:822–826, 2017.

[8] J. Wagner, V. Haigis, D. Kunzel, and S. Jahn. Trace element partitioning between silicate melts - a molecular dynamics approach. *Geochim. Cosmochim. Acta*, 205:245–255, 2017.

[9] C. J. L. de Grouchy, C. Sanloup, B. Cochain, J. W. E. Drewitt, Y. Kono, and C. Crépisson. Lutetium incorporation in magmas at depth: changes in melt local environment and the influence on partitioning behaviour. *Earth Planet. Sci. Lett.*, 464:155–165, 2017.

[10] P. C. Piilonen, F. Farges, R. L. Linnen, G. E. Brown, M. Pawlak, and A. Pratt. Structural

environment of Nb^{5+} in dry and fluid-rich (H_2O, F) silicate glasses: A combined XANES and EXAFS study. *Can. Mineral.*, 44:775–794, 2006.

[11] A. D. Burnham, A. J. Berry, B. J. Wood, and G. Cibin. The oxidation states of niobium and tantalum in mantle melts. *Chem. Geol.*, 330–331:228–232, 2012.

[12] C. Cartier, T. Hammouda, M. Boyet, O. Mathon, D. Testemale, and B. N. Moine. Evidence for Nb^{2+} and Ta^{3+} in silicate melts under highly reducing conditions: A XANES study. *Am. Mineral.*, 100:2152–2158, 2015.

[13] R. A. Mayanovic A. J. Anderson W. A. Bassett and I.-M. Chou. Synchrotron x-ray spectroscopy of Eu/HNO_3 aqueous solutions at high temperatures and pressures and Nb-bearing silicate melt phases coexisting with hydrothermal fluids using a modified hydrothermal diamond anvil cell and rail assembly. *Rev. Sci. Instr.*, 78:053904, 2007.

[14] O. Mathon, A. Beteva, J. Borrel, D. Bugnazet, D. Gatla, R. Hino, I. Kantor, T. Mairs, M. Munoz, S. Pasternak, F. Perrin, and S. Pascarelli. The time-resolved and extreme conditions XAS (TEXAS) facility at the European Synchrotron Radiation Facility: the general-purpose EXAFS bending-magnet beamline BM23. *J. Synchrotron Radiat.*, 22:1548–1554, 2015.

[15] G. Shen, H.-P. Liermann, S. Sinogeikin, W. Yang, X. Hong, C.-S. Yoo, and H. Cynn. Distinct thermal behavior of GeO_2 glass in tetrahedral, intermediate, and octahedral forms. *Proc Natl Acad Sci USA*, 104:14576–14579, 2007.

[16] N. Ishimatsu, Kawamura N., M. Mizumaki, H. Maruyama, H. Sumiya, and T. Irifune. Applications of nano-polycrystalline diamond anvils to X-ray absorption spectroscopy under high pressure. *High Press. Res.*, 36:381–390, 2016.

[17] Y. Fei, J. Li, K. Hirose, W. Minarik, J. Van Orman, C. Sanloup, W. van Westrenen, T. Komabayashi, and K. i. Funakoshi. A critical evaluation of pressure scales at high temperatures by in situ x-ray diffraction measurements. *Phys. Earth Planet. Int.*, 143:515–526, 2004.

[18] B Ravel and M Newville. ATHENA, ARTEMIS, HEPHAESTUS: data analysis for X-ray absorption spectroscopy using IFEFFIT. *J. Synchrotron Rad.*, 12(4):537–541, 2005.

[19] M. Newville. EXAFS analysis using FEFF and FEFFIT. *J. Synchrotron Radiat.*, 8:96–100, 2001.

[20] M. Newville, B. Ravel, D. Haskel, J. J. Rehr, E. A. Stern, and Y. Yacoby. Analysis of multiple-scattering XAFS data using theoretical standards. *Physica B Condens. Matter.*, 208–209:154–156, 1995.

[21] F. Farges, C. W. Ponader, and G. E. Brown. Structural environments of incompatible elements in silicate glass/melt systems: I. Zirconium at trace levels. *Geochim. Cosmochim. Acta*, 55:1563–1574, 1991.

[22] F. Farges and S. Rossano. Water in Zr-bearing synthetic and natural glasses. *Eur. J. Mineral.*, 12:1093–1107, 2000.

[23] F. Farges, G. E. Brown, P.-E. Petit, and M. Munoz. Transition elements in water-bearing silicate glasses/melts. Part I. a high-resolution and anharmonic analysis of Ni coordination environments in crystals, glasses, and melts. *Geochim. Cosmochim. Acta*, 65:1665–1678, 2001.

[24] M. Wilke. Fe in magma - an overview. *Annals Geophysics*, 48:609–617, 2005.

[25] D. Manuel, Cabaret D., C. Brouder, P. Sainctavit, A. Bordage, and N. Trcera. Experimental evidence of thermal fluctuations on the x-ray absorption near-edge structure at the aluminum K edge. *Phys. Rev. B*, 85:224108, 2012.

[26] F Farges. Does Zr-F 'complexation' occur in magmas? *Chem. Geol*, 127(4):253–268, 1996.

[27] X. Xiong, H. Keppler, A. Audétat, H. Ni, W. Sun, and Y. Li. Partitioning of Nb and Ta between rutile and felsic melt and the fractionation of Nb/Ta during partial melting of hydrous metabasalt. *Geochim. Cosmochim. Acta*, 75:1673–1692, 2011.

[28] G.D. Bromiley and S.A.T. Redfern. The role of tio_2 phases during melting of subduction-modified crust: Implications for deep mantle melting. *Earth Planet. Sci. Lett.*, 267:301–308, 2008.

[29] T. Imai, E. Takahashi, T. Suzuki, and H. Takafumi. Element partitioning between olivine and melt up to 10 GPa: Implications for the effect of pressure. *Phys. Earth Planet. Int.*, 212:64–75,

2012.